IEEE Access
Multidisciplinary ⋮ Rapid Review ⋮ Open Access Journal

Received 28 July 2022, accepted 22 August 2022, date of publication 29 August 2022, date of current version 8 September 2022.

Digital Object Identifier 10.1109/ACCESS.2022.3202537

RESEARCH ARTICLE

Sensitive and Robust Millimeter-Wave/Terahertz Photonic Crystal Chip for Biosensing Applications

YIXIONG ZHAO[1,2], JAN-HENDRIK BUCHHOLZ[3], THORBEN GRENTER[1], XUAN LIU[2], GERD VOM BÖGEL[1], KARSTEN SEIDL[1,4], (Member, IEEE), AND JAN C. BALZER[2]

[1]Fraunhofer Institute for Microelectronic Circuits and Systems (IMS), 47057 Duisburg, Germany
[2]Chair of Communication Systems (NTS), Faculty of Engineering, University of Duisburg-Essen (UDE), 47057 Duisburg, Germany
[3]University of Duisburg-Essen (UDE), 47057 Duisburg, Germany
[4]Department of Electronic Components and Circuits and Center for Nanointegration Duisburg-Essen (CENIDE), University of Duisburg-Essen, 47057 Duisburg, Germany

Corresponding author: Yixiong Zhao (yixiong.zhao@uni-due.de)

This research was Funded by the Deutsche Forschungsgemeinschaft (DFG, German Research Foundation) – Project-ID 287022738 – TRR 196. We acknowledge support by the Open Access Publication Fund of the University of Duisburg-Essen.

ABSTRACT In recent years terahertz (THz) technology has attracted great interest in biosensing applications. Due to the interaction between analyte and electromagnetic (EM) field, a THz resonator is sensitive to changes in the refractive index of the analyte and can be used as a thin-film sensor for rapid pathogen diagnosis. To achieve high sensitivity and reliability, the sensor should have a high Q factor, a high field concentration at the site of the analyte, and the ability to compensate for temperature effects. However, conventional metamaterial methods have a low Q factor, which may lead to ambiguous detection and no attention has been paid to address the temperature effects. Here, we present a photonic crystal (PhC) based chip consisting of a reference channel and a sensing channel with two identical PhC slot resonators. The resonance difference between the resonators is temperature invariant and can be used for analyte detection. The dual-channel PhC chip has a Q factor of 5063 and a figure of merit of 3.1 /RIU/μm (RIU is refractive index unit), which are higher than that of metamaterial sensors. The chip is designed and simulated for the W band by 3D field simulations and is verified by measurements. Our results suggest that THz PhC resonators can provide high sensitivity and high resistance to environmental effects. We anticipate our work to be a starting point for future biosensing applications.

INDEX TERMS High Q factor, photonic crystal resonator, temperature invariant, terahertz, thin-film sensing.

I. INTRODUCTION

Millimeter wave/terahertz (THz) radiation, falling between microwave and infrared band, has emerged as a hot topic for sensing applications due to its characteristics such as low photo energy for nondestructive detection [1] and small wavelength for high resolution imaging [2]. Of particular interest is the thin-film sensor for biosensing applications [3]. To detect pathogen detection applications, target pathogens, such as bacteria, can be bonded to specific sites with specific antibodies, forming a monolayer with a thickness in the micrometer range on the sensor surface [4]. The interaction between the thin-film analyte and electromagnetic (EM) field makes it possible to detect the change in the refractive index and the volume of the analyte [3]. A challenge is how to achieve a reliable sensing capacity with only a small amount of analyte.

THz metamaterial-based sensors are a widely studied method. Current research focuses on achieving a high Q factor to facilitate detection and enhancing the field concentration. Taleb *et al.* fabricated a free-standing metamaterial resonator with an asymmetric structure leading to a Fano resonance with a Q factor of 29 [5]. Singh *et al.* demonstrated a metamaterial based on quadrupole and Fano resonances with

The associate editor coordinating the review of this manuscript and approving it for publication was San-Liang Lee.

a Q factor of 65 [6]. The metamaterial sensors can be easily characterized by spectrometers. However, the Q factor is still limited due to high radiation losses and the resonance shift is small compared to the full width at half maximum (FWHM), which may lead to ambiguous detection. To increase the confinement of the waves and reduce radiation losses, all-dielectric photonic crystal (PhC) methods are investigated. Cheng *et al.* demonstrated a PhC cavity structure with a Q factor of 529 for thin-film sensing [7]. However, a high-level alignment is required and the free-space measurement has high path loss. Islam *et al.* presented a porous core PhC fiber for chemical sensing [8] and a squared hollow-core PhC fiber sensor for protein detection [9]. The PhC fiber has the advantages of high confinement and low propagation attenuation along the fiber. However, it is not clear how to bind the pathogen in the fiber and the field concentration is lower than for resonant methods. Furthermore, Ju *et al.* fabricated a 3-dimensional PhC structure using direct writing technology for liquid sensing [10]. But a resonant structure with a high interaction between EM waves and the analyte is difficult to achieve.

Okamot *et al.* showed a PhC slab resonator at 318 GHz with a Q factor of 10800, which can detect 5 μm thick dielectric polyester tape [11]. Compared with the other approaches, the PhC slab resonator has high field concentration at the resonance frequency, high transmission efficiency through a waveguide-coupled measurement setup, mature fabrication technology, and the ease to immobilize the analyte on its surface. However, although a high Q factor has been achieved, little attention has been paid to the interaction between electric field and the analyte. The electric field is mostly concentrated within the silicon of the PhC resonator, while the analyte is only captured on the surface of the resonator. This leads to a weak interaction and lowers the sensitivity of the sensor [12]. Furthermore, few researchers have addressed environmental effects. The refractive index and the physical dimension of the fabricated material varies with temperature, which leads to a shift of the resonance frequency [13]. For reliable measurements, a reference or a stable temperature is required.

In this paper, we present a sensitive and reliable PhC sensor chip consisting of two channels with individual resonators. The resonators have a slot in the middle to achieve a strong interaction between the analyte und electric field and were optimized for a high Q factor and a high sensitivity to a micrometer thin layer of the analyte. The two channels with the resonators work as a sensing channel and a reference channel to eliminate the influence of the temperature and simplify the measurement. The sensing capacities of the single resonator and the dual-channel sensor chip were analyzed using the EM simulation tool CST Microwave Studio. To validate the design, a single PhC slot resonator and a dual-channel PhC sensor chip for sub-THz frequencies were fabricated with a laser-cutting technique for fast prototyping. They were experimentally characterized with sodium chloride (NaCl) as analyte.

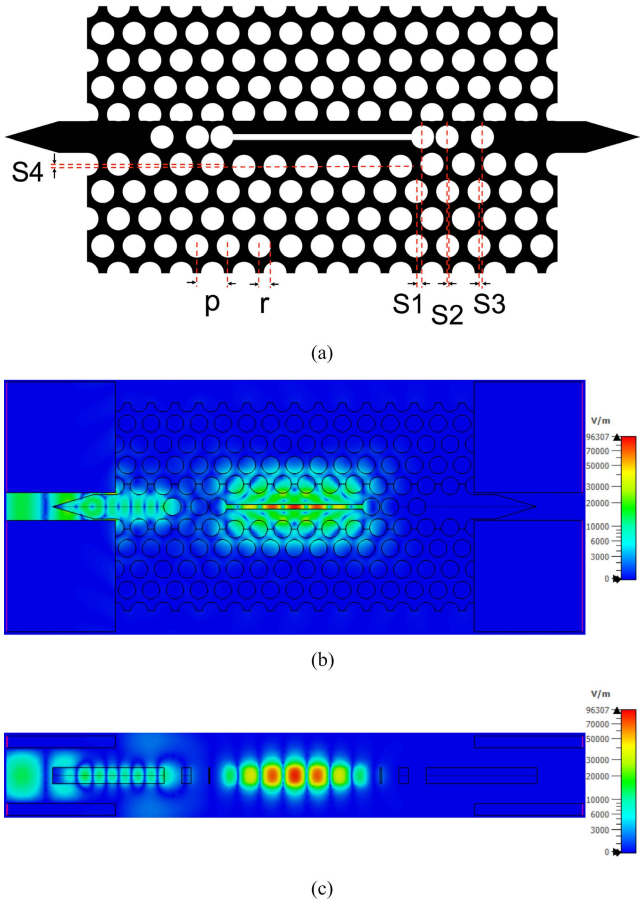

FIGURE 1. The single PhC slot resonator: (a) layout; (b) electric field distribution in the horizontal direction at the resonance frequency $f_r = 91.108$ GHz; (c) electric field distribution in the vertical direction in the air slot at the resonance frequency $f_r = 91.108$ GHz. The field amplitude is color coded.

This article is organized as follows: In Section 2, we present the structure design and simulation results of the single resonator and the dual-channel sensor chip. In Section 3, the fabrication and the experimental setup are described. Section 4 presents the measurement results in terms of sensitivity and temperature dependence. Section 5 contains the conclusions.

II. STRUCTURE DESIGN AND SIMULATION

A. STRUCTURE DESIGN

To achieve a high sensitivity and a high Q factor, a PhC resonator with a slot in the middle is firstly designed as shown in Fig. 1 (a). Based on this design, a PhC chip consisting of two channels with the slot resonator in each channel is proposed as shown in Fig. 2 (a). They are based on a PhC slab with a triangular lattice of air holes in a high-resistivity silicon (HRSi) slab, which can be easily fabricated by micro- and nanotechnology. HRSi is used because of its low loss (loss tangent = 0.00015) and high permittivity of 11.68 in THz regime [14]. EM waves are reflected at each air/silicon interface and interfere with each other. This leads to a suppression of waves in a

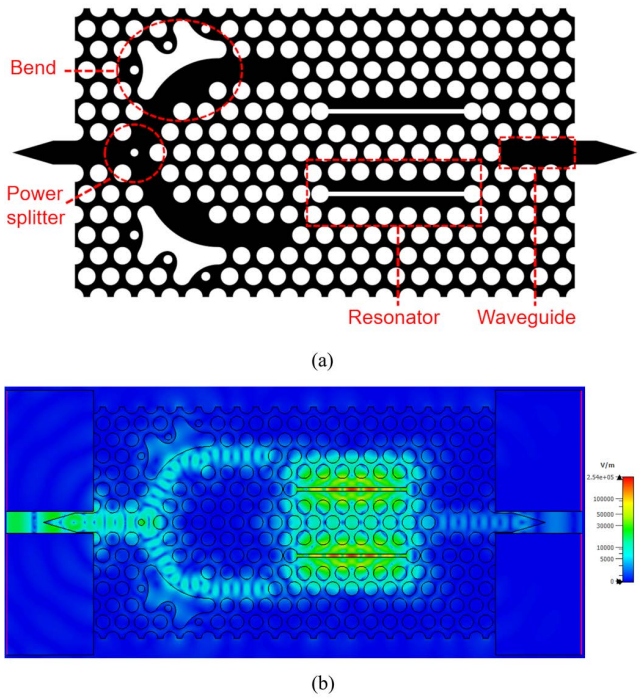

FIGURE 2. The dual-channel PhC sensor chip: (a) layout; (b) electric field distribution at the resonance frequency $f_r = 91.130$ GHz. The field amplitude is color coded.

certain frequency range, which is called bandgap frequency. The bandwidth of the bandgap frequency is broad due to the high contrast of the permittivity of air and silicon [15]. Within the bandgap frequency, waves can be confined to a region by removing air holes. Thus, waveguides and resonators can be realized, as shown in Fig. 2 (a).

To optimize the design efficiently, simulations in CST were carried out. In the simulation setup, a frequency solver was used to get rapid and precise results for the resonance. Frequency samples to sweep were set to automatic type. A tetrahedral mesh type with adaptive mesh refinement was chosen. The boundaries were set to open boundary conditions, which extends the touching geometry virtually to infinity by using a perfectly matched layer (PML) boundary. As in real experiments, WR10 rectangular metallic waveguides were created in CST for energy excitation and reception. The waveguide dimensions were 1.27 mm in height and 2.54 mm in width, ensuring single-mode operation in the 75 GHz to 110 GHz frequency range. Two waveguide ports were connected to the WR10 waveguides to simulate the S-parameters for the TE10 mode.

Since an intuitive relationship between dimensions and resonance frequency and Q factor, respectively, is not found, the photonic crystal slab is studied with numerical tools by sweeping structural dimensions [16]. In our work, the layouts were designed iteratively in CST. In every step, we swept the dimensions and observe the S parameters and electric field distribution. After the desired properties were found, we swept the dimensions with a finer step width to search the optimum performance. Based on this guideline, we design the resonator step by step: (a) finding an optimum photonic crystal design, (b) building a resonator by removing holes, (c) introducing a slot, and (d) shifting the holes near the resonator to achieve an optimum Q factor.

We started to design the single slot resonator with the goal to achieve a high Q factor and a high field concentration in the slot. Three parameters define the PhC slab: the lattice period p (the distance between the centers of two adjacent holes), the radius of the holes r, and the thickness of the slab t. These parameters determine the center frequency and the bandwidth of the bandgap [15]. Considering the cost effectiveness for the later fabrication, a standard HRSi wafer with a thickness of $t = 725\mu m$ was used. Hence, only the parameters p and r were optimized in CST for maximum bandgap bandwidth. For $p = 1100\mu m$ and $r = 400\mu m$, a bandgap which covers 75 GHz to 110 GHz was found. In a second step, 5 holes were removed in the center of the PhC slab to obtain a resonator with a high Q factor [17]. Because the resonator has the largest field concentration in the silicon, where the analyte under test cannot be placed, the interaction between the analyte and electric field is limited. To enhance the interaction and improve thus the sensitivity, a slot is introduced in the middle of the resonator. Now, the maximum electric field is in the air-filled slot as shown in Fig. 1 (b). Thus, the thin film analyte can be placed on the wall of the slot for detection.

The Q factor of the slot resonator depends on radiation losses, coupling losses with waveguides, and material losses [15]. Among them, the radiation losses make the largest contribution. Moving the adjacent holes around the resonator can adjust electric field profile and reduce the radiation losses [17]. In this work, the first and the third adjacent holes along the resonator were shifted towards the outside with a displacement of S1 and S3, respectively. The second hole was shifted towards the inside with a displacement of S2 as shown in Fig. 1 (a). The holes below and above the resonator were shifted towards the outside with a displacement of S4. The displacements of the holes and the width of the slot were optimized in CST to achieve the maximum Q factor. The optimized S1, S2, S3, S4 and the width of the slot are 219 μm, 50 μm, 120 μm, and 197 μm, respectively. As the next step, waveguides and tapers were designed for excitation and detection of the resonator. The waveguides were realized by removing holes in a line. A short distance between the waveguides and the resonator favors a strong coupling. This leads to a high transmission magnitude but a low Q factor. Here, the waveguides were placed three holes away from the resonator as a trade-off between good coupling and a high Q factor. To save space, the waveguides were aligned with the resonator. Then, a taper transition connected to the waveguide was built for the sake of minimal reflection and efficient energy coupling between the PhC waveguides and the WR10 rectangular metallic waveguides. The taper consists of a straight silicon waveguide with the same width as

the PhC waveguides and a taper with a continuous transition. Their lengths were chosen as 1 mm and 2 mm, respectively, for good transitions and robustness in fabrication and experiments. While the taper is not required for the simulation, it is important for the experiments where a WR10 waveguide-coupled network analyzer will be used. Fig. 1 (b) depicts the electric field at the resonance frequency $f_r = 91.108$ GHz. Waves are coupled from the WR10 waveguide through the PhC waveguide to the resonator where a standing wave pattern arises. The resonance frequency is highly sensitive to a variation in permittivity around the resonator, which is used for analyte detection. Furthermore, the electric field distribution in the vertical direction in the air slot is shown in Fig. 1 (c). The electric field is maximum in the center of the resonator and decreases in the direction perpendicular to the plate. The decay length to the half maximum is 427 μm.

While the sensitivity problem is solved by introducing a slot into the resonator, the temperature dependence is still critical with respect to the reliability of the measurements. Hence, we use the optimized resonator to design a PhC chip with two channels to eliminate the effect of temperature variations. The PhC sensor chip consists of a power divider, two bends, two channels with a slot resonator, and a power combiner, as shown in Fig. 2 (a). First, the power splitter divides the EM waves from the WR10 waveguide equally into two channels as illustrated in Fig. 2 (b). A small hole with a diameter of 175 μm was introduced in the center of the splitter to improve impedance matching and transmission efficiency [18]. Second, the waves flow through the 60° bend to alter propagation direction. A round opening was introduced along the bend to guide the wave with low radiation losses [19]. The diameter of the three holes near the opening were adjusted to 200 μm. Third, the waves in the two channels are coupled through three rows of holes into two identical slot resonators, respectively. Finally, the waves are combined at the output PhC waveguide. Because both slot resonators have an identical design, they show the same response to temperature variation. Hence, the outputs of both channels interfere constructively at the output. For detection of the analyte, one of them is kept empty and serves as the reference channel, while the other is loaded with the analyte and serves as the sensing channel. The analyte causes a resonance shift of the sensing channel, which leads to a second detectable resonance frequency at the output. The difference frequency between the resonances should be temperature independent and relate to the permittivity of the analyte.

B. SIMULATION WITH ANALYTE

The designed single resonator and the dual-channel sensor chip were simulated with an analyte of varying refractive index n and varying thickness h_a to analyze their sensing performance. As mentioned in the introduction, thin film sensors are of great interest for the diagnosis of pathogens. Target pathogens, such as bacteria or virus, can be captured by specific antibodies on the sensor surface and dried by heating [3] or N_2 injection [20]. As a result, a monolayer of the captured bacteria forms a thin film with a thickness in the micrometer range and changes refractive index on the sensor surface.

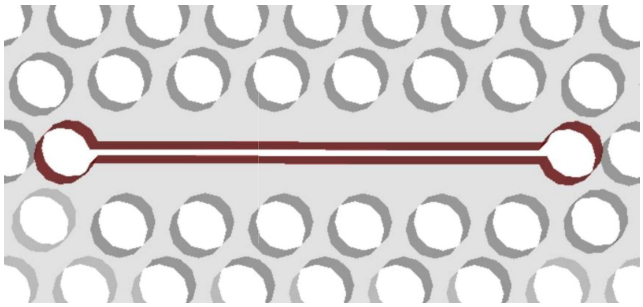

FIGURE 3. Model of the analyte on the wall of the slot in the resonator.

The effect of the analyte on the resonance frequency can be explained using the perturbation theory. Here, it is assumed that the perturbated EM field can be approximated by the unperturbed EM field, since the volume of the analyte is much smaller than the resonator. The resonance shift Δf_r due to the analyte can be expressed by [15]:

$$\frac{\Delta f_r}{f_r} \approx -\frac{\Delta n}{n} \cdot \frac{\iiint V_a dV \varepsilon \left|\vec{E}\right|^2}{\iiint V_0 dV \varepsilon \left|\vec{E}\right|^2}, \tag{1}$$

where V_a is the volume of the resonator and V_0 is the volume of the whole area including the resonator, the analyte, and the surrounding air. It can be seen that the fractional change in resonance frequency is related to the fractional change in refractive index and the fraction of the electric field energy in the analyte. The minus symbol means that increasing in refractive index and the volume of the analyte result in decreasing the resonance frequency.

The thin film analyte was modeled in CST and covers the wall of the slot of the resonator as shown in Fig. 3. Because the thickness of the PhC slab $t = 725\mu m$ is much larger than the thickness of the film, errors may occur during the simulation. For a reliable result, the thin film analyte was set as an independent mesh with fine mesh step width in the local mesh properties. According to the results in [21], the real part of the permittivity of different bacteria ranges from 2.75 to 4.11 at 1 THz. In our simulation, the refractive index n of the analyte was changed from 1.0 (air) to 2.0 to simulate the empty and analyte-loaded resonator.

First, the transmission parameter S21 of the resonator was simulated with $h_a = 0.5\mu m$ and a variation of n from 1.0 to 2.0 as shown in Fig. 4 (a). The empty resonator ($n = 1.0$) has a resonance frequency of $f_r = 91.108$ GHz as shown in Fig. 4 (a) (black line). The FWHM of the unloaded resonator is 14.4 MHz. The Q factor is calculated to be 6327 by using the expression [11]:

$$Q = f_r / \mathbf{FWHM}. \tag{2}$$

With the increasing n, the transmission spectrum shifts to lower frequencies as expected from (1). Since the volume

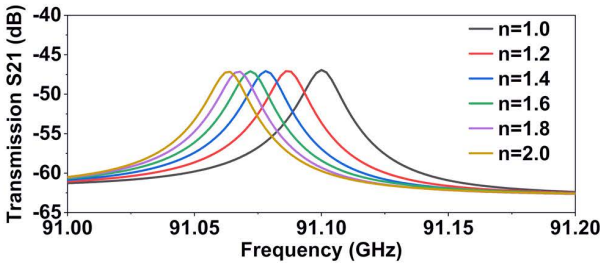

(a)

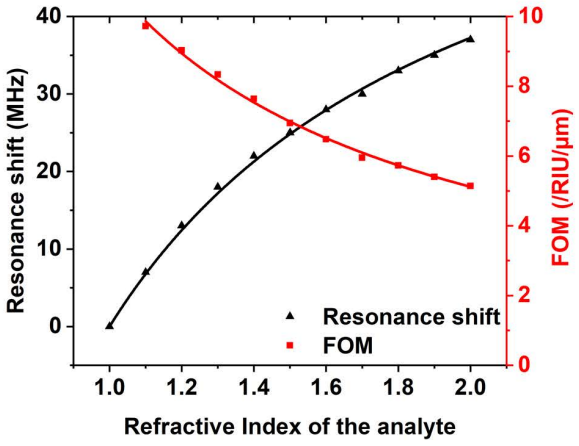

(b)

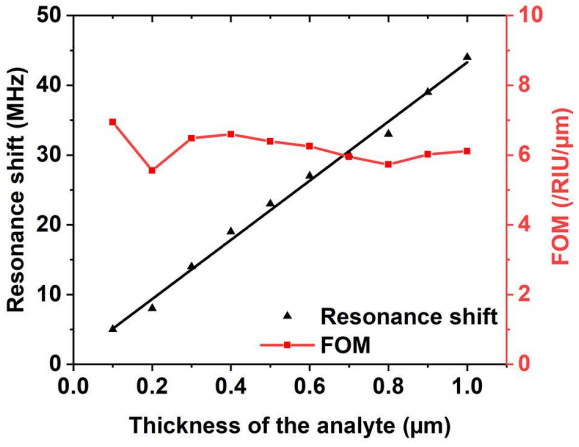

(c)

FIGURE 4. Simulation results of the single PhC resonator: (a) the transmission parameter S21 with varying refractive index of the thin film analyte; (b) the resonance shift and the FOM with varying refractive index; (c) the resonance shift and the FOM with varying thickness of the thin film analyte.

of the analyte is much smaller than the resonator and the change in refractive index is small, it can be assumed that the electric field distribution does not change and the fraction of the electric field energy is constant. Thus, (1) can be approximated by $\Delta f_r = -A \cdot (n-1)/n$, where A is a constant. Fig. 4 (b) shows the resonance shift with varying refractive index and was fitted using this equation. Its coefficient of determination (COD) is 0.9985, which shows the resonance shift has a reciprocal relation to n as expected. To evaluate overall sensing performance for the thin film analyte, a figure-of-merit (FOM) parameter regarding the unit thickness of the analyte is defined as [3]:

$$\mathbf{FOM} = \Delta f_r \big/ (\mathbf{FWHM} \cdot \Delta n \cdot h_a). \tag{3}$$

The FOM of the resonator with varying n is plotted in Fig. 4 (b), where RIU is the refractive index unit. With (1), the FOM can be expressed as

$$\mathbf{FOM} \approx \frac{Q}{n \cdot h_a} \cdot \frac{\iiint V_a dV \varepsilon \left|\vec{E}\right|^2}{\iiint V_0 dV \varepsilon \left|\vec{E}\right|^2}. \tag{4}$$

Similar to the resonance shift with varying n, the FOM can also be fitted using a reciprocal curve with a COD of 0.9968. The FOM decreases from 9.7 /RIU/μm to 5.1 /RIU/μm as n increase from 1.1 to 2.0. It shows a high FOM compared to the results of the THz metamaterial biosensor in [5] (0.6 /RIU/μm) and [22] (0.3 /RIU/μm).

We further investigate the effects of the analyte's thickness by sweeping h_a from 0.1 μm to 1 μm while keeping $n = 1.5$ constant. The resonance shift increases with increasing h_a as shown in Fig. 4 (c). In this case, the volume of the analyte V_a increases linearly with increasing h_a. Since V_a is much smaller than V_0, it is assumed that the electric field distribution is the same as the unperturbed field and the electric field does not change along the thickness in the analyte. As a results, the integration in the nominator is linearly related to the thickness and the integration in the denominator is constant. Then, (1) can be approximated by $\Delta f_r = B \cdot h_a$, where B is a constant. The resonance shift with varying h_a can be linearly fitted with a COD of 0.9941. Its COD is smaller than that in the simulation with varying n, because the mesh of the analyte can change with h_a in spite of the setup of the independent mesh. As a result, the calculated FOM is between 5.6 /RIU/μm and 6.9 /RIU/μm. With the slope of the resonance shift with varying thickness, the average FOM is calculated to be 5.8 /RIU/μm.

Second, the PhC chip with two channels was investigated by loading one resonator with the analyte as the sensing channel and keeping the other resonator empty as the reference channel. The transmission parameter S21 was simulated with $h_a = 0.5\mu m$ and a variation of n from 1.0 to 2.0 as shown in Fig. 5 (a). The frequency spectrum for $n = 1.0$ shows that the empty chip has only one resonance at 91.130 GHz with an FWHM of 18 MHz. The Q factor is calculated to be 5063, which is lower than that of the single resonator. The reason is that the coupling between the waveguide and the resonator of the two-channel sensor chip is stronger than in the single resonator, which leads to higher coupling losses and a higher transmission at the resonance frequency. The resonance frequency of the sensing resonator is shifted to a lower frequency. From $n = 1.2$, the S21 parameter starts to show two peaks: one peak with a lower frequency $f_{r,l}$

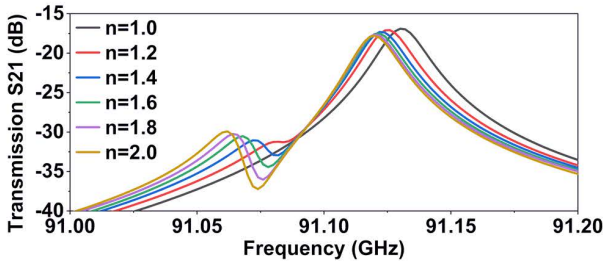

(a)

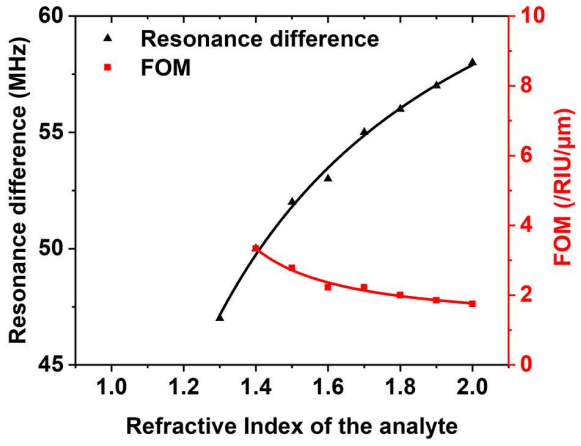

(b)

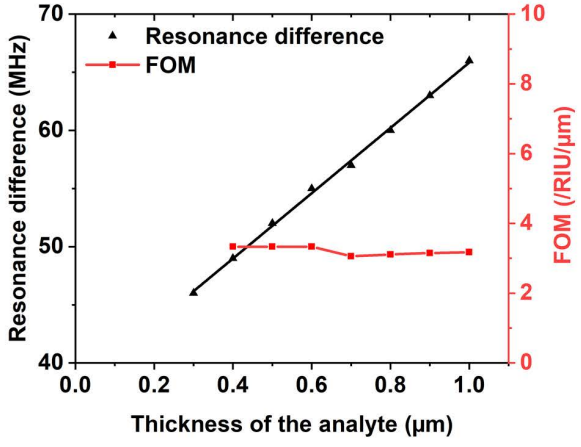

(c)

FIGURE 5. Simulation results of the dual-channel PhC sensor chip: (a) the transmission parameter S21 with varying refractive index of the thin film analyte; (b) the resonance difference and the FOM with varying refractive index; (c) the resonance difference and the FOM with varying thickness of the thin film analyte.

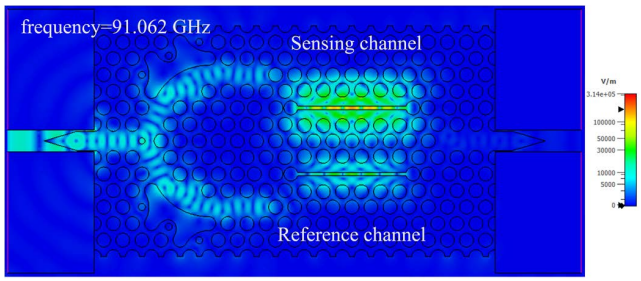

(a)

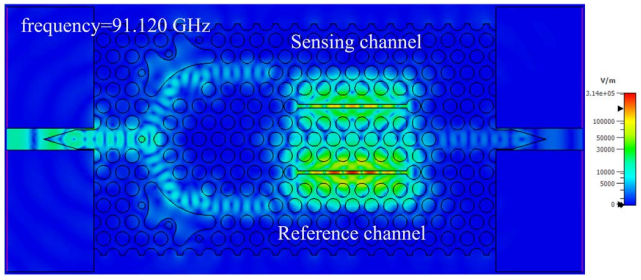

(b)

FIGURE 6. Electric field distribution of the dual-channel sensor chip with a thin film analyte with a thickness of 0.5 μm and refractive index of 2.0 at: (a) $f_{r,l}$= 91.062 GHz; (b) $f_{r,h}$= 91.120 GHz.

which is related to the detuned sensing resonator and the other peak with a higher frequency $f_{r,h}$ which is related the reference resonator. Fig. 6 (a) and (b) show the electric field distribution at $f_{r,l} = 91.062$ GHz and $f_{r,h} = 91.120$ GHz, respectively, for $n = 2.0$. The upper resonator is in both cases the sensing resonator. The sensing resonator has a strong oscillation at $f_{r,l}$, while the reference resonator has a strong oscillation at $f_{r,h}$. Fig. 5 (a) shows that the amplitude at $f_{r,l}$ is greatly reduced, while the amplitude of the peak at $f_{r,h}$ is similar to that of the empty chip and $f_{r,h}$ is slightly shifted to lower frequencies. As n increases, $f_{r,l}$ shifts further to lower frequencies and the amplitude increases slightly. This is due to interference between the two resonators through the air holes and the PhC waveguides [23]. As the refractive index of the analyte increases, the resonance frequency of the sensing resonator is further reduced and the interference gets weaker. As a result, the amplitude at $f_{r,l}$ increases. The interference is difficult to eliminate in passive components with a small footprint. However, the resonance difference between $f_{r,l}$ and $f_{r,h}$ can be easily used for analyte detection. Additionally, the difference frequency of the two resonances is temperature independent as both resonators act identically to a temperature change.

Fig. 5 (b) shows the resonance difference with varying n. For $n < 1.3$ the resonance peak at $f_{r,h}$ is not separated and the resonance difference cannot be plotted. The resonance difference increases as n increases. Similarly, the resonance difference is fitted using a reciprocal function with a COD of 0.9960 and the FOM is fitted using a reciprocal function with a COD of 0.9830. The FOM ranges from 1.7 /RIU/μm to 3.3 /RIU/μm, which is smaller than that of the single resonator. The reason is that the decreased Q factor and the interference between the two resonators depress the FOM. However, to guarantee that the sensing resonator and the reference resonator react to the temperature in the same manner, their resonance frequency are designed identical. In addition, the dependence on the analyte thickness was investigated by sweeping h_a from 0.1 μm to 1 μm while

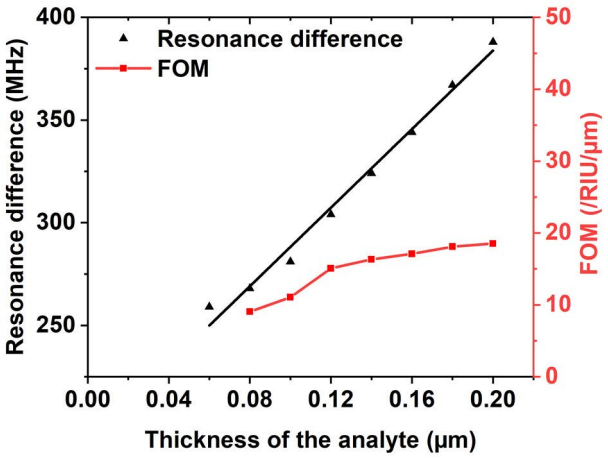

FIGURE 7. Simulation results of the scaled dual-channel PhC sensor chip at 500 GHz: the resonance difference and the FOM with varying thickness of the thin film analyte.

keeping n= 1.5 constant. Similar as the single resonator, the resonance difference is linearly correlated to h_a and the FOM keeps almost constant as shown in Fig. 5 (c). The calculated FOM is between 3.1 /RIU/μm and 3.3 /RIU/μm. With the slope of the resonance shift, the average FOM is calculated to be 3.1 /RIU/μm. The FOM of the chip is still high compared with other sensors and this compact chip provides a simple reference measurement for analyte detection.

C. SCALED CHIP AT 500 GHz

Our design is based on a standard HRSi wafer with a thickness of 725 μm for cost efficiency. The thickness of the wafer determines the operating frequency of the PhC so that the designed resonator is at about 90 GHz. In fact, the chip is a passive component and can be scaled to the THz frequency range for thin-film sensing. To prove this, the chip was scaled to 500 GHz to study its FOM. Correspondingly, the dependence on the analyte thickness was investigated by sweeping h_a from 0.02 μm to 0.2 μm while keeping n= 1.5 constant. Fig. 7 shows the simulated resonance difference and the FOM with varying h_a. It can be noted that the resonance differences are much higher than that of the 90 GHz chip even for thinner analyte. The FOM ranges from 9.0 /RIU/μm to 18.5 /RIU/μm and is hence improved compared to the 90 GHz device. The results reveal that the proposed PhC chip will work in THz range with an improved sensing capacity.

III. EXPERIMENT SETUP

A. FABRICATION

As mentioned above, we choose a standard 725 μm thick HRSi wafer with a resistivity higher than 10 kΩcm for prototyping due to its low cost. During fabrication, the HRSi wafer was cut by a high energy laser for fast prototyping. The production was carried out by a waterjet-laser system. The system combines the advantages of laser cutting and waterjet cutting by processing the workpiece with an infrared fiber laser and an ultrafine waterjet simultaneously. This process makes it possible to produce parts accurately without damaging the material and provide high surface quality of the inner sides of the cut holes. Structures larger than 30 μm with a height-to-width ratio of up to 400:1 can be produced with high accuracy. A precision of +/- 1 μm is given from the manufacturer. Fig. 8 (a) and (b) show the fabricated single resonator and dual-channel sensor chip, respectively.

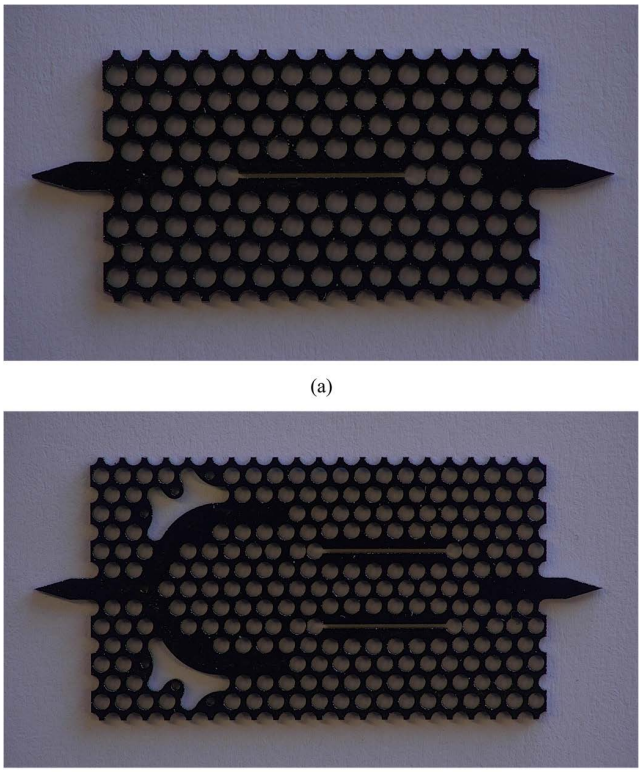

FIGURE 8. Fabrication: (a) the single PhC resonator; (b) the dual-channel PhC sensor chip.

B. ANALYTE PREPARATION

To investigate the sensing performance of the fabricated resonator and chip, NaCl was used as the analyte. NaCl can be easily resolved in water and washed off from the wall of the slot in the resonator, so that the resonator can be reused for the experiments. Furthermore, NaCl is easy to handle, and a high-level biological lab is not needed. Dry NaCl was resolved in distilled water to prepare NaCl solutions with different concentration (1, 2, 3, 5 and 10 μg/μL). In the experiments, 2 μL of the prepared solution were transferred using a pipette. The solution was slowly dropped into the two holes connected to the slot to prevent the liquid leaking to other places and let the liquid flow into the slot. According to our observation, the solution stays inside the slot and dries on the walls. After the solution dried, only the NaCl stays on the walls with a weight of 2, 4, 6, 10 and 20 μg on the resonator, respectively. After

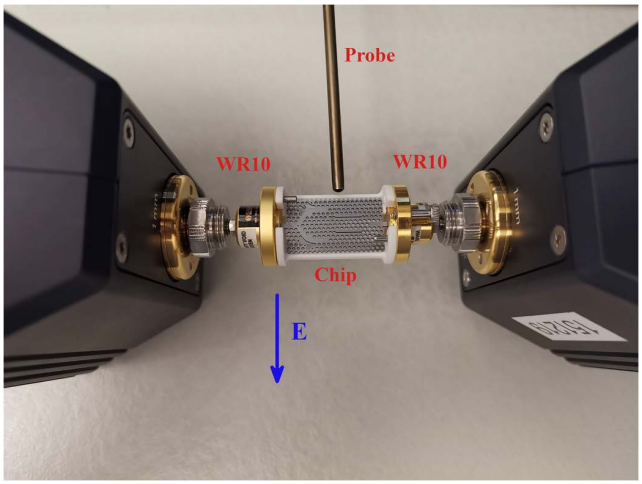

FIGURE 9. Measurement setup: the chip was connected by WR10 waveguides and thermometer probe was placed close to it.

each measurement, the resonator and the chip were washed using water.

C. MEASUREMENT SETUP

To characterize the resonance frequency, a Keysight PNA-X network analyzer N5247B was used. A Keysight millimeter test set N5292A, two Keysight broadband frequency extenders N5295 and two WR10 rectangular metallic waveguide adapters were connected for W band (75 GHz – 110 GHz) measurements. The electric field from the waveguide is horizontally polarized as shown in Fig. 9. The chip was mounted by a 3-D printed support made of Polyamid 12 as shown in Fig. 9. The input and output tapers of the chip were inserted into the WR10 waveguides for excitation and detection, respectively. The transmission parameter S21 was measured to observe the resonance peak. The frequency resolution was set to 500 KHz as a trade-off between accuracy and measurement speed. Before the measurements, the device is calibrated using through waveguide, offset waveguide and short termination. However, stochastic errors of the measurements cannot be eliminated. To reduce the noise of the measurements, the averaging function and the smoothing function of the network analyzer were used. Each curve was averaged from 10 scans and smoothed by computing a moving average over 1% of the trace. The range was set to 200 MHz centered at 92.05 GHz. To characterize the temperature dependence of the resonance frequency, the chip was heated using a hot air heat gun. The temperature of the heat gun and the distance between the heater and chip were adjusted to heat the chip to different temperatures. The temperature was measured using a probe of a thermometer placed near to the chip as shown in Fig. 9.

IV. MEASUREMENT RESULTS

A. SENSITIVITY OF THE SINGLE RESONATOR

To investigate the relationship between the shift in resonance frequency and the amount of the analyte, the single

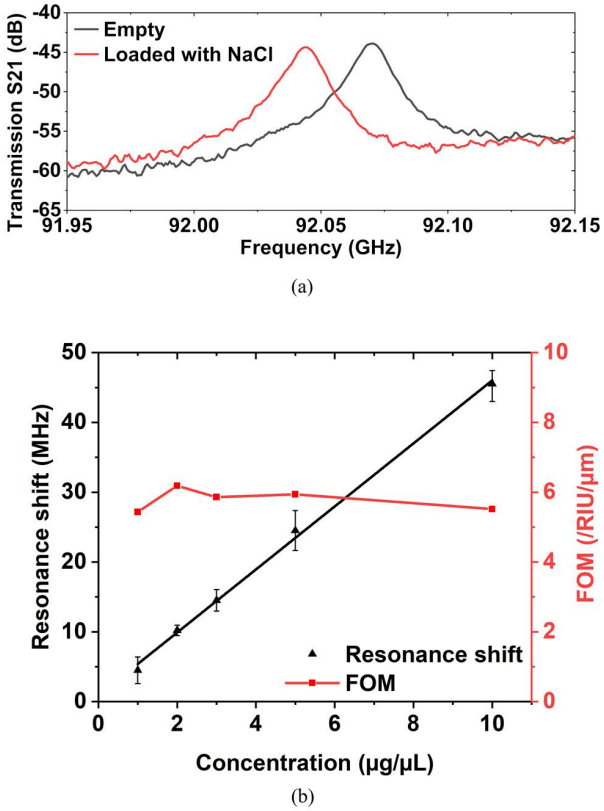

FIGURE 10. Measurement results of the fabricated single resonator: (a) the transmission parameter S21 without NaCl and with NaCl; (b) the resonance shift and the FOM with varying concentration.

resonator was characterized with different concentration of NaCl solution as mentioned above. First, the single resonator was connected to the network analyzer and the transmission parameter S21was measured at room temperature. Then, 2 μL of the prepared NaCl solution was dropped in the slot of the resonator using a pipette. A decrease of the maximum S21 was observed which is due to losses in the water. As the drop dries, the transmission increases. The drying of the drop ends when the S21 parameter becomes static. At this point, the S21 parameter was recorded. After that, the resonator was washed with water to remove the dried NaCl and was dried to perform the next measurement. This procedure was repeated 5 times for each concentration of the solution and the mean value of the measurement was calculated to minimize random effects. An example measurement result from the single resonator for a concentration of 5 ug/μL is shown in Fig. 10 (a). The empty resonator has a resonance frequency of 92.070 GHz with a FWHM of 15 MHz, which is in good agreement with the simulated results. The Q factor was calculated to be 6138. The loading of the dried NaCl results in a shift of the resonance frequency.

The measured resonance shift increases with increasing concentration as shown in Fig. 10 (b). As explained for the simulation results with varying thickness of the analyte, the electric field distribution is assumed to be unchanged in

the whole area and constant along the thickness of the analyte, since the volume of the analyte is much smaller than the resonator. As a result, the resonance shift is linearly related to the electric field energy in the volume of the analyte. If the NaCl is uniformly distributed on the wall of the slot, the resonance shift is linearly related to the volume or the thickness of the NaCl. The linear relationship is shown in the simulation results with varying thickness of the analyte in Fig. 4 (c). On the other side, the measurement results with varying concentration shows a high linearity. The measured resonance shift with varying concentration can be linearly fitted with a slope of 4.5 MHz/(μg/μL) and a COD of 0.9974. The volume of the analyte is linearly corelated to the concentration as expressed:

$$V_a = V_{drop} \cdot C/\rho, \tag{5}$$

where V_{drop} is the volume of one drop of the solution, C is the concentration and ρ is the density of dry NaCl. If the NaCl is assumed to be uniformly distributed on the wall, the thickness is linearly corelated to the volume as expressed:

$$h_a = V_a/S, \tag{6}$$

where S is the area of the slot surface as shown in Fig. 3. The thickness of the NaCl on the wall of the slot is calculated to be 0.1, 0.2, 0.3, 0.5 and 1 μm for the concentration 1, 2, 3, 5 and 10 μg/μL, respectively. The high linearity of the measured resonance shift and low standard deviation (smaller than 2.9 MHz) shows that the uniform distribution of the NaCl is an appropriate assumption to characterize the sensing capacity of the resonator for thin-film analytes. The sensitivity to the concentration can be calculated for the sensitivity to the weight or the thickness of the NaCl, which are 2.25 MHz/μg or 45 MHz/μm, respectively. Furthermore, the refractive index of dry NaCl was estimated to be 1.55 according to the measurement in [24]. With this estimation, the FOM is between 5.4 /RIU/μm and 6.2 /RIU/μm as shown in Fig. 10 (b). With the slope of the resonance shift, the average FOM is calculated to be 5.1 /RIU/μm, which agrees with the simulated FOM (5.8 /RIU/μm). The limit of detection (LOD) of the resonator sensor can be defined as the minimum amount of analyte that leads to a resonance shift that corresponds to the FWHM. According to the measurement results, 7.1 μg or 0.35 μm thin NaCl corresponds to the LOD. The standard deviation of the frequency shift ranges between 0.7 MHz and 2.9 MHz, which may have two reasons. The first is due to tolerances in the manual liquid transfer, such as the volume of the transferred solution, the exact position of the placed solution, and non-uniform distribution of the dried NaCl, which cannot be avoided. The second is due to temperature variations in the environment and system noise.

B. SENSITIVITY OF THE DUAL-CHANNEL SENSOR CHIP

The resonance difference of the dual-channel sensor chip was characterized using the same measurement procedure as for the single resonator. The only difference was that only the sensing resonator in the chip was loaded with the

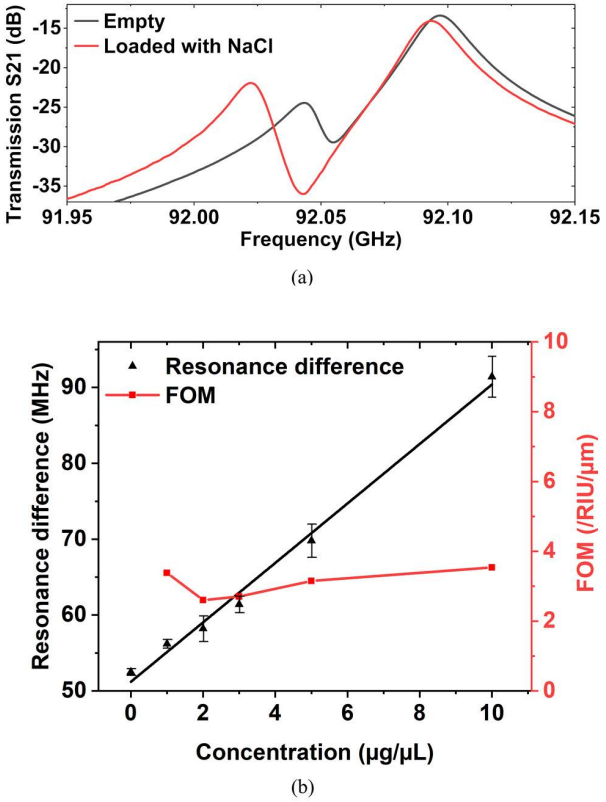

FIGURE 11. Measurement results of the fabricated dual-channel sensor chip: (a) the transmission parameter S21 without NaCl and with NaCl; (b) the resonance difference and the FOM with varying concentration.

NaCl, while the reference resonator of the chip was kept empty. A measurement result of the chip without the NaCl (empty) and with dried NaCl from 2 μL of the solution with a concentration 5 ug/μL is depicted in Fig. 11 (a). The empty chip shows two resonance peaks: $f_{r,l}$ = 92.045 GHz and $f_{r,h}$ = 92.098 GHz. The FWHM at $f_{r,h}$ is 20 MHz and the Q factor is 4604. The reason, why two resonance peaks in the transmission spectrum are present can be attributed to the fabrication tolerance of the resonators. In particular, the width of the slots plays a major role in the resonance frequency. However, the resonance differences can still be used for the analyte detection. Loading the sensing channel with NaCl causes a shift of the lower resonance frequency $f_{r,l}$ and an increase in amplitude as expected from the simulations.

Fig. 11 (b) shows the measured resonance differences, which are linearly related to the concentration. The slope of the linear fit is 3.9 MHz/(μg/μL). This corresponds to 1.95 MHz/μg or 39 MHz/μm of dry NaCl. The standard deviation of the resonance differences ranges between 0.5 MHz and 2.7 MHz. With the estimation of the refractive index of dry NaCl n = 1.55, the calculated FOM is between 2.6 /RIU/μm and 3.5 /RIU/μm as shown in Fig. 11 (b). With the slope of the resonance difference, the average FOM is calculated to be 3.5 /RIU/μm, which agrees with the simulated FOM (3.1 /RIU/μm). It is noted that the measured FOM is slightly higher than the simulated FOM. One reason can be

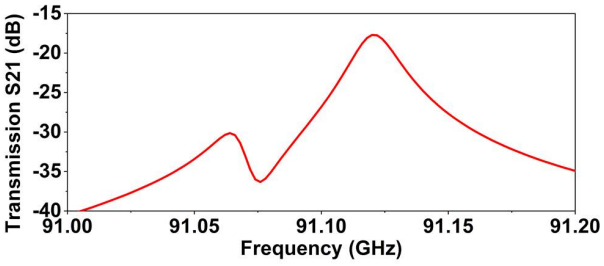

(a)

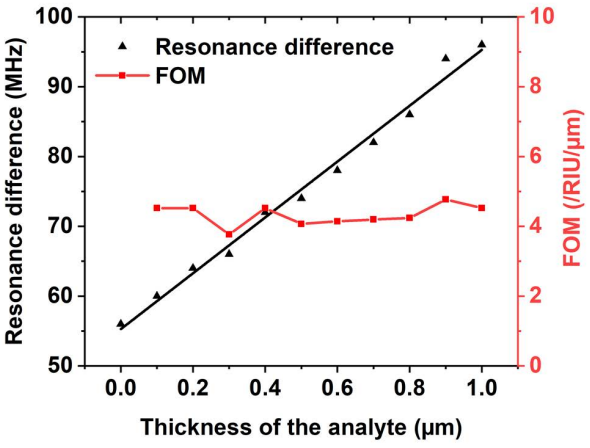

(b)

FIGURE 12. Simulation results of the dual-channel PhC sensor chip with two different resonators: (a) the transmission parameter S21 of the empty chip; (b) the resonance difference and the FOM with varying thickness of the thin film analyte.

that the resonance frequencies of both resonators of the fabricated chip are slightly different, resulting in weaker interference compared to the situation with identical resonators. The reduced interference improves the sensitivity. To prove this, a chip with two different resonators is simulated. The reference resonator has a slot width of 197 μm, while the sensing resonator has a slot width of 196.4 μm. As shown in Fig. 12 (a), the simulated transmission parameter has two resonance peaks at 91.12 GHz and 91.064 μm, respectively. Its sensing capacity was investigated by sweeping h_a from 0.1 μm to 1 μm while keeping n= 1.5 constant as shown in Fig. 12 (b). The calculated FOM is between 3.8 /RIU/μm and 4.5 /RIU/μm and the average FOM is 4.4 /RIU/μm, which are higher than the simulated FOM of the chip with two identical resonators. Due to the tolerance in manufacturing, it was observed that the sensitivity can be increased by varying the resonance frequencies of the two resonators. In future works the effect of the resonance difference on the interference and the sensitivity will be investigated in more detail. Furthermore, the LOD of the chip is calculated to be 10.3 μg or a 0.51 μm thin NaCl film.

C. TEMPERATURE DEPENDENCE

To investigate the temperature dependence, the single resonator and dual-channel sensor chip were heated with an

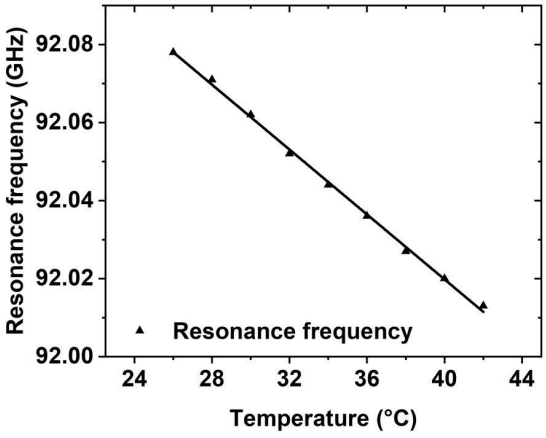

(a)

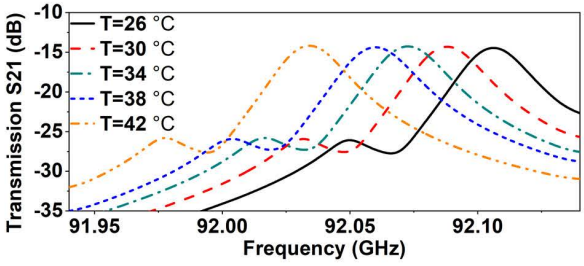

(b)

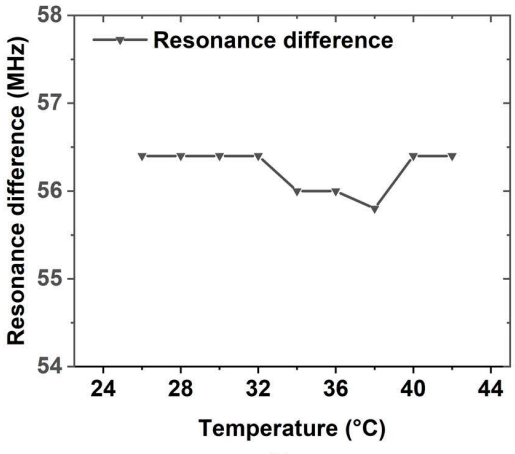

(c)

FIGURE 13. Temperature dependences: (a) the resonance frequency of the single resonator with varying temperature; (b) the transmission parameter S21 of the dual-channel sensor chip with varying temperature; (c) the resonance difference of the dual-channel sensor chip with varying temperature.

air heater. The temperature was measured by placing a thermal probe near to the chip and recording the measured temperature as shown in Fig. 9. The distance between the heater and chip was adjusted to heat the chip to temperatures from 26 to 42 °C. The measured resonance frequency of the single resonator decreases linearly as the temperature increases as shown in Fig. 13 (a). This can be attributed to the change in the refractive index and the thermal

expansion of the silicon [25]. The slope of the fitted line is -4.1 MHz/°C. Fig. 13 (b) shows the transmission parameter of the dual-channel chip for increasing temperature. Both resonance peaks shift to lower frequency in the same manner. The resonance differences between both resonance frequencies are calculated and plotted in Fig. 13 (c). The resonance difference is constant with varying temperature. It can be observed that the loaded chip has a constant resonance difference of 56.4 MHz, where only three of the performed measurements show a deviating behavior with a maximum deviation of only 0.6 MHz. This indicates that the chip consisting of the reference channel and the sensing channel is mostly invariant to the temperature of the chip. Using this chip, strict temperature control is not required and the resonance difference can be easily read for analyte detection.

V. CONCLUSION AND FUTURE WORKS

In this work, we proposed a PhC chip with two channels with slot resonators for thin film sensing. The slot resonator was designed for a high field concentration in the slot and a high Q factor, which improves the sensitivity. The proposed chip consists of a sensing channel and a reference channel to suppress influences of the environmental temperature. The resonance difference of the resonators can be used for analyte detection. In the simulation, the single resonator has a FOM of 5.8 /RIU/μm and shows a high sensitivity compared to THz metamaterial sensors in [5] (0.6 /RIU/μm) and [22] (0.3 /RIU/μm). The resonance difference of the dual resonator design has a FOM of 3.1 /RIU/μm due to the lower Q factor and the interference between the two resonators. They were fabricated with rapid prototyping technique using laser cutting. In the experiments, NaCl was used as analyte, which is easy to prepare and to clean and does not require special treatment or laboratory equipment. The single resonator shows a LOD of 7.1 μg or 0.35 μm thin NaCl, and the Chip has a LOD of 10.3 μg or 0.51 μm thin NaCl. Furthermore, the temperature dependency was investigated. The resonance frequency of the resonator is linearly correlated with the temperature, while the resonance difference of the chip is almost temperature invariant. The high sensitivity and the robustness to the environment ensure a reliable detection of an ultrathin analyte film.

Our works indicates that the proposed PhC chip has high potential for biosensing applications. First, the PhC resonator shows a high field concentration and a high Q factor which leads to a high sensitivity and FOM. Second, the compact chip consisting of two channels suppresses negative influences due to the ambient temperature. Third, the PhC chip can be easily mass-produced from silicon to reduce costs. Furthermore, the silicon chip can be easily coupled with rectangular waveguides and has the potential to integrate with THz sources and detectors [26] which will reduce the measurement setup complexity and size. In future works, we will investigate the effect of the resonance difference on the interference and the sensitivity. Moreover, a microfluidic channel can be integrated with the chip to eliminate the tolerances of bringing the analyte to the sensor. Additionally, it will be interesting to test other rapid prototyping methods with high permittivity materials such as ceramic 3-D printing [27].

REFERENCES

[1] A. Soltani, S. F. Busch, P. Plew, J. C. Balzer, and M. Koch, "THz ATR spectroscopy for inline monitoring of highly absorbing liquids," *J. Infr., Millim., THz Waves*, vol. 37, no. 10, pp. 1001–1006, Oct. 2016, doi: 10.1007/s10762-016-0285-6.

[2] D. Damyanov, I. Willms, J. C. Balzer, B. Friederich, M. Yahyapour, N. Vieweg, A. Deninger, K. Kolpatzeck, X. Liu, A. Czylwik, and T. Schultze, "High resolution lensless terahertz imaging and ranging," *IEEE Access*, vol. 7, pp. 147704–147712, 2019, doi: 10.1109/ACCESS.2019.2934582.

[3] M. Beruete and I. Jáuregui-López, "Terahertz sensing based on metasurfaces," *Adv. Opt. Mater.*, vol. 8, no. 3, pp. 1–26, 2020, doi: 10.1002/adom.201900721.

[4] T. J. Günther, M. Suhr, J. Raff, and K. Pollmann, "Immobilization of microorganisms for AFM studies in liquids," *RSC Adv.*, vol. 4, no. 93, pp. 51156–51164, 2014, doi: 10.1039/c4ra03874f.

[5] F. Taleb, I. Al-Naib, and M. Koch, "Free-standing complementary asymmetric metasurface for terahertz sensing applications," *Sensors*, vol. 20, no. 8, p. 2265, Apr. 2020, doi: 10.3390/s20082265.

[6] R. Singh, W. Cao, I. Al-Naib, L. Cong, W. Withayachumnankul, and W. Zhang, "Ultrasensitive terahertz sensing with high-*Q* Fano resonances in metasurfaces," *Appl. Phys. Lett.*, vol. 105, no. 17, Oct. 2014, Art. no. 171101, doi: 10.1063/1.4895595.

[7] W. Cheng, Z. Han, Y. Du, and J. Qin, "Highly sensitive terahertz fingerprint sensing with high-*Q* guided resonance in photonic crystal cavity," *Opt. Exp.*, vol. 27, no. 11, p. 16071, May 2019, doi: 10.1364/oe.27.016071.

[8] M. S. Islam, J. Sultana, K. Ahmed, M. R. Islam, A. Dinovitser, B. W. H. Ng, and D. Abbott, "A novel approach for spectroscopic chemical identification using photonic crystal fiber in the terahertz regime," *IEEE Sensors J.*, vol. 18, no. 2, pp. 575–582, Jan. 2018, doi: 10.1109/JSEN.2017.2775642.

[9] M. A. Islam, M. R. Islam, A. M. A. Naser, F. Anzum, and F. Z. Jaba, "Square structured photonic crystal fiber based THz sensor design for human body protein detection," *J. Comput. Electron.*, vol. 20, no. 1, pp. 377–386, Feb. 2021, doi: 10.1007/s10825-020-01606-2.

[10] X. Ju, W. Yang, S. Gao, and Q. Li, "Direct writing of microfluidic three-dimensional photonic crystal structures for terahertz technology applications," *ACS Appl. Mater. Interfaces*, vol. 11, no. 44, pp. 41611–41616, Nov. 2019, doi: 10.1021/acsami.9b10561.

[11] K. Okamoto, K. Tsuruda, S. Diebold, S. Hisatake, M. Fujita, and T. Nagatsuma, "Terahertz sensor using photonic crystal cavity and resonant tunneling diodes," *J. Infr., Millim., THz Waves*, vol. 38, no. 9, pp. 1085–1097, Sep. 2017, doi: 10.1007/s10762-017-0391-0.

[12] Y. Zhao, K. Vora, X. Liu, G. V. Bögel, K. Seidl, and J. C. Balzer, "Photonic crystal resonator in the millimeter/terahertz range as a thin film sensor for future biosensor applications," *J. Infr., Millim., THz Waves*, pp. 1–19, Jun. 2022, doi: 10.1007/s10762-022-00859-1.

[13] A. Jimenez-Saez, M. Schusler, D. Pandel, C. Krause, Y. Zhao, G. V. Bogel, N. Benson, and R. Jakoby, "Temperature characterization of high-*Q* resonators of different materials for mm-wave indoor localization tag landmarks," in *Proc. 14th Eur. Conf. Antennas Propag. (EuCAP)*, Mar. 2020, pp. 3–7, doi: 10.23919/EuCAP48036.2020.9135861.

[14] A. Jiménez-Sáez, M. Schubler, C. Krause, D. Pandel, K. Rezer, G. V. Bogel, N. Benson, and R. Jakoby, "3D printed alumina for low-loss millimeter wave components," *IEEE Access*, vol. 7, pp. 40719–40724, 2019, doi: 10.1109/ACCESS.2019.2906034.

[15] J. D. Joannopoulos, S. G. Johnson, J. N. Winn, and R. D. Meade, *Photonic Crystals: Molding the Flow of Light*, 2nd ed. Princeton, NJ, USA: Princeton Univ. Press, 2008.

[16] M. Minkov and V. Savona, "Automated optimization of photonic crystal slab cavities," *Sci. Rep.*, vol. 4, no. 1, pp. 1–8, May 2015, doi: 10.1038/srep05124.

[17] T. Asano and S. Noda, "Photonic crystal devices in silicon photonics," *Proc. IEEE*, vol. 106, no. 12, pp. 2183–2195, Dec. 2018, doi: 10.1109/JPROC.2018.2853197.

[18] S. Boscolo, M. Midrio, and T. F. Krauss, "Y junctions in photonic crystal channel waveguides: High transmission and impedance matching," *Opt. Lett.*, vol. 27, no. 12, p. 1001, Jun. 2002, doi: 10.1364/ol.27.001001.

[19] E. G. Turitsyna and S. Webb, "Simple design of FBG-based VSB filters for ultra-dense WDM transmission," *Electron. Lett.*, vol. 41, no. 2, pp. 40–41, 2005, doi: 10.1049/el:20056760.
[20] Z. Geng, X. Zhang, Z. Fan, X. Lv, and H. Chen, "A route to terahertz metamaterial biosensor integrated with microfluidics for liver cancer biomarker testing in early stage," *Sci. Rep.*, vol. 7, no. 1, pp. 1–11, Dec. 2017, doi: 10.1038/s41598-017-16762-y.
[21] S. A. Yoon, S. H. Cha, S. W. Jun, S. J. Park, J.-Y. Park, S. Lee, H. S. Kim, and Y. H. Ahn, "Identifying different types of microorganisms with terahertz spectroscopy," *Biomed. Opt. Exp.*, vol. 11, no. 1, p. 406, Jan. 2020, doi: 10.1364/boe.376584.
[22] C. Zhang, T. Xue, J. Zhang, L. Liu, J. Xie, G. Wang, J. Yao, W. Zhu, and X. Ye, "Terahertz toroidal metasurface biosensor for sensitive distinction of lung cancer cells," *Nanophotonics*, vol. 11, no. 1, pp. 101–109, Dec. 2021, doi: 10.1515/nanoph-2021-0520.
[23] K. Nozaki, A. Shinya, S. Matsuo, T. Sato, E. Kuramochi, and M. Notomi, "Ultralow-energy and high-contrast all-optical switch involving Fano resonance based on coupled photonic crystal nanocavities," *Opt. Exp.*, vol. 21, no. 10, p. 11877, May 2013, doi: 10.1364/oe.21.011877.
[24] C. Liu, L. Zhang, J. Peng, W. Qu, B. Liu, H. Xia, and J. Zhou, "Dielectric properties and microwave heating characteristics of sodium chloride at 2.45 GHz," *High Temp. Mater. Processes*, vol. 32, no. 6, pp. 587–596, Dec. 2013, doi: 10.1515/htmp-2013-0008.
[25] B. J. Frey, D. B. Leviton, and T. J. Madison, "Temperature-dependent refractive index of silicon and germanium," *Proc. SPIE*, vol. 6273, Jun. 2006, Art. no. 62732J, doi: 10.1117/12.672850.
[26] R. A. S. D. Koala, M. Fujita, and T. Nagatsuma, "Nanophotonics-inspired all-silicon waveguide platforms for terahertz integrated systems," *Nanophotonics*, vol. 11, no. 9, pp. 1–19, 2022, doi: 10.1515/nanoph-2021-0673.
[27] J. Ornik, M. Sakaki, M. Koch, J. C. Balzer, and N. Benson, "3D printed Al_2O_3 for terahertz technology," *IEEE Access*, vol. 9, pp. 5986–5993, 2021, doi: 10.1109/ACCESS.2020.3047514.

YIXIONG ZHAO received the B.Sc. degree in electrical engineering from the Beijing Institute of Technology, China, in 2012, and the M.Sc. degree in information and communication technology from RWTH Aachen, Germany, in 2017. Since 2018, he has been working with the Fraunhofer Institute for Microelectronic Circuits and Systems. His main research interests include terahertz biosensor and RFID technologies.

JAN-HENDRIK BUCHHOLZ received the B.Sc. degree in electrical engineering and information technology and the M.Sc. degree in communications engineering from the University of Duisburg-Essen, Germany, in 2018 and 2021, respectively. During his master's studies, he has been working as a Student Research Assistant at the Fraunhofer Institute for Microelectronic Circuits and Systems. Since 2021, he has been employed as a Researcher and a Development Engineer at IMST GmbH, Kamp-Lintfort, Germany, where he concentrates on radio frequency technology and communication systems.

THORBEN GRENTER received the B.S. and M.S. degrees in electrical engineering and information technology from TU Dortmund, in 2015 and 2018, respectively. He joined the Fraunhofer Institute for Microelectronic Circuits and Systems, in 2018, and took the Lead of the Group of Wireless Sensors and Systems, in 2022. His main research interests include wireless sensors, novel RFID technologies for harsh environments, and signal processing for wireless systems.

XUAN LIU received the B.S. degree in electrical and electronic engineering and the M.S. degree in communications engineering from the University of Duisburg-Essen, Germany, in 2015 and 2017, respectively, where she is currently pursuing the Ph.D. degree in electrical engineering and information technology with the Department of Communication Systems (NTS). Her current research interests include the development and investigation of dielectric THz passive components and the study of beamforming concepts for THz frequencies.

GERD VOM BÖGEL received the Diploma degree in electrical engineering and the Dr.-Ing. degree from the University of Duisburg, in 1992 and 1999, respectively. He joined the Fraunhofer Institute for Microelectronic Circuits and Systems, Duisburg. At present, he is responsible for the business unit of transponder and RF systems at the Fraunhofer Institute IMS. His main research interests include energy harvesting and sensor transponder systems.

KARSTEN SEIDL (Member, IEEE) received the Dr.-Ing. degree from the University of Freiburg/IMTEK, Germany. From 2012 to 2018, he was with Robert Bosch and Bosch Healthcare Solutions (BHCS) GmbH. He is currently a Professor for micro- and nanosystems for medical technology with the University of Duisburg-Essen. He has been the Head of Business Field Health with the Fraunhofer Institute for Microelectronic Circuits and Systems, Duisburg, Germany, since 2018.

JAN C. BALZER received the Dipl.-Ing. (FH) degree in telecommunications from the University of Applied Sciences, Dortmund, Germany, in 2008, and the M.Sc. degree in electrical engineering and information technology and the Ph.D. degree in electrical engineering for the work on ultrafast semiconductor lasers from the Ruhr-Universität Bochum, Bochum, Germany, in 2010 and 2014, respectively. In 2015, he joined with the Group of Prof. Martin Koch, Philipp-Universität Marburg, Marburg, Germany, as a Postdoctoral Research Fellow. Since 2017, he has been an Assistant Professor with the Faculty of Engineering, University of Duisburg-Essen, Germany, where he combines his knowledge of ultrafast semiconductor lasers with his expertise in system building of THz spectrometers. His main research interest includes THz technology and its application.